Analysis of temperature field for a surface-mounted and interior permanent magnet synchronous motor adopting magnetic-thermal coupling method

Jikai Si, Suzhen Zhao, Haichao Feng, Yihua Hu, and Wenping Cao

***Abstract*—Aiming at obtaining high power density of surface-mounted and interior permanent magnet synchronous motor (SIPMSM), it is important to accurately calculate the temperature field distribution of SIPMSM, and a magnetic-thermal coupling method is proposed. The magnetic-thermal coupling mechanism is analyzed. The thermal network model and finite element model are built by this method, respectively. The effects of power frequency on iron losses and temperature fields are analyzed by the magnetic-thermal coupling finite element model under the condition of rated load, and the relationship between the load and temperature field is researched under the condition of the synchronous speed. In addition, the equivalent thermal network model is used to verify the magnetic-thermal coupling method. Then the temperatures of various nodes are obtained. The results show that there are advantages in both computational efficiency and accuracy for the proposed coupling method, which can be applied to other permanent magnet motors with complex structures.**

***Index Terms*—Equivalent thermal network method, magnetic-thermal coupling method, power frequency, iron loss, surface-mounted and interior permanent magnet synchronous motor(SIPMSM), temperature field.**

I. Introduction

SURFACE-MOUNTED and interior permanent magnet synchronous motor (SIPMSM) integrates the advantages of over load ability, high power density, high efficiency and energy saving presented in surface mounted and interior permanent magnet motor[1-2]. As the power density of SIPMSM increases, its unit volume loss increases, along with the operation temperature. Many insulation materials are included in SIPMSM, whose performances are directly related to the motor temperature. The temperature of SIPMSM also directly affects the working point of permanent magnet, and excessively high temperature may damage the insulation materials and lead to irreversible demagnetization of the permanent magnet. It can eventually lead to performance indicators decline and the SIPMSM may even stop working [3]. Therefore, it is important and necessary to accurately estimate the temperature distribution of the SIPMSM during the process of motor design.

The hybrid rotor structure of surface-mounted permanent magnet (SPM) and interior permanent magnet (IPM) is adopted by SIPMSM. After a SIPMSM works for a long period of time, the temperature will sharply rise because of the eddy current loss in the permanent magnet and poor thermal conduction ability of the rotor. Therefore, larger deviation at the working point of permanent magnet is induced, and then the back EMF produced by it is changed, which influences the distribution of the internal magnetic field of SIPMSM, resulting in increased losses. The transformation of the working point of permanent magnet affects not only the magnetic flux densities in the air gap and core, but also the amplitude of the current required to produce the same torque. Thus, along with the change of the temperature of the permanent magnet, iron loss and winding copper loss will change. In addition, the winding copper loss and the size of the permanent magnet eddy current loss are related to the conductivity of the change with temperature. Therefore, it is necessary to propose a new method to accurately predict the temperature distribution of SIPMSM.

The analysis of the temperature field of the motor is mainly used the concentrated heat parameter method, equivalent thermal network method and finite element method [4-8]. The finite element method is becoming popular to exactly calculate the real temperature distribution of each component of the motor [9-12]. The literatures [13-18] base on the coupling of flow field and temperature field, the mathematical model and physical model are established, and the finite element method is used to calculate the coupling field. The correctness of the proposed model is verified by the temperature test of motor.

This article was submitted for review on 05, September, 2017.

This work was supported by Natural Science Foundation of China (Item number: 51777060, U1361109) and Natural Science Foundation of Henan province (Item number: 162300410117) and the he innovative research team plan of Henan Polytechnic University (Item number: T2015-2).

Jikai Si is with School of Electrical Engineering and Automation, Henan Polytechnic University, Jiaozuo, China. (e-mail: sijikai527@126.com)

Suzhen Zhao is with School of Electrical Engineering and Automation, Henan Polytechnic University, Jiaozuo, China.(e-mail:18236883396@163.com)

Haichao Feng is with School of Electrical Engineering and Automation, Henan Polytechnic University, Jiaozuo, China. (e-mail: fhc@hpu.edu.cn)

Yi-Hua Hu is with Department of Electrical Engineering and Electronics, University of Liverpool, Liverpool, UK. (e-mail: Y.Hu35@liverpool.ac.uk)

Wenping Cao is with School of Electronics, Electrical Engineering and Computer Science, Queen's University Belfastd, Northern Ireland, UK. (e-mail: w.cao@qub.ac.uk)

The literature [19] aims to the multi-physics field coupling problem in the segment of the submersible motor, and it establishes a coupling model of electromagnetic-force-thermal, and the accuracy of the calculation the finite element method is proved by comparing with the experimental results. The temperature field of SIPMSM about another kind of structural form is presented [20], and the three-dimensional finite element method is used to analyze the 3-D full-domain temperature field of SIPMSM.

Therefore, this paper adopts the finite element method and numerical method to calculate the temperature field distribution of the SIPMSM, and puts forward analysis of the mechanism of magnetic-thermal coupling. In order to accurately estimate the temperature of each part of SIPMSM, the magnetic-thermal coupling method is used to calculate the temperature distribution. The finite element model and equivalent thermal network model of magnetic-thermal coupling are established to study the magnetic-thermal coupling mechanism of SIPMSM, and calculate the temperature distribution in the rated operation state. The relationship between the power frequency and temperature distribution in the rated load and that between the load and temperature fields at the synchronous speed are analyzed. The proposed method can be used to predict the temperature distribution of hybrid permanent magnet motors.

II. Structure of SIPMSM and Mechanism Analysis

A. Structure and parameters of SIPMSM

SIPMSM contains surface-mounted permanent magnet (SPM) and interior permanent magnet (IPM), Fig.1 shows the structure of SIPMSM and the corresponding key design parameters are shown in Table I.

TABLE I
THE PARAMETERS OF SIPMSM

Items	Value/ unit
Number of pole	4
Number of turns	41
Air gap length	0.5mm
Axial length	135mm
Rated current	12.2A
Rated voltage	380V
Rated power	7.5kW
Inner diameter of the stator	91mm
Outer diameter of the stator	155mm
Thickness of the permanent magnet	2mm

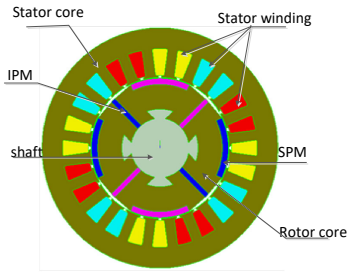

Fig. 1. The structure diagram of SIPMSM.

B. Mechanism analysis

The magnetic-thermal coupling mechanism of SIPMSM is that the iron losses, copper losses and permanent magnet eddy current losses are produced in the motor, which affects the temperature field distribution. The magnetic field of SIPMSM is generated by the permanent magnet excitation. When the working point of the permanent magnet is influenced by the temperature, the distribution of the magnetic field inside the motor is influenced by the permanent magnet, and the magnetic flux density in the air gap and the core will change. The iron losses and permanent magnet eddy current losses are affected by the magnetic field. The thermal conductivity, the resistance of the copper core, the permanent magnet remanence and intrinsic coercivity are affected by the temperature.

The relationships between the copper losses, iron losses, permanent magnet eddy current losses and temperature are shown in formulas (1) - (4) respectively[21].

$$P_{\mathrm{cu}} = 3\mathrm{I}^2 R \tag{1}$$

$$P_{Fe} = K_e f^2 B^2 + K_h f B^2 \tag{2}$$

$$P_{PM} = \frac{\sigma_{PM}\pi^2}{6} V_{PM} f_{PM} w_{PM}^2 B_{PM}^2 \tag{3}$$

$$\frac{P_{cu} + P_{Fe} + P_{PM}}{V} = -\lambda\left(\frac{\partial^2 T}{\partial x^2} + \frac{\partial^2 T}{\partial y^2} + \frac{\partial^2 T}{\partial z^2}\right) \tag{4}$$

Where I is the current effective value of a phase winding coil. R is the phase winding resistance. f is the alternating magnetization frequency. K_e , K_h are respectively the eddy current loss and hysteresis loss coefficient, and B is the maximum flux density motivated by AC power. σ_{PM} is the permanent magnet conductivity, V_{PM} is the volume of permanent magnet, f_{PM} is the eddy current frequency in permanent magnet, w_{PM} is the span of permanent magnet along the rotor circumferential direction, B_{PM} is the amplitude of magnetic flux density in permanent magnet. T is the temperature, V is the volume of the motor, λ is the thermal conductivity.

The relational expressions between the temperature and iron core thermal conductivity, copper resistance, remanence and intrinsic coercivity respectively of the permanent magnet can be illustrated in formula (5) - (8)[22].

$$R_t = \frac{234.5 + T_t}{234.5 + T_o} R_0 \tag{5}$$

$$\lambda_t = \lambda_0 \left(1 + \alpha T_t\right) \tag{6}$$

$$B_{rt} = B_{r0}\left(1 - \frac{s}{100}\right)\left[1 - \frac{\alpha_{Br}}{100}\left(T_t - T_0\right)\right] \tag{7}$$

$$\alpha_{H_{ct}} = \frac{H_{ct} - H_{c0}}{H_{c0}\left(T_t - T_0\right)} * 100 \tag{8}$$

Where T_0 is the initial temperature, T_t is the temperature at t , R_0 is the resistance at T_0, R_t, is the resistance at T_t, is the iron core thermal conductivity at T_t, λ_0 is the iron core thermal conductivity at T_0, α is the iron core temperature coefficient, B_{ro} and B_{rt} are respectively the residual magnetic flux density at T_0 and T_t, α_{Br} is the permanent magnet remanence that is reversely related to temperature, s is the percentage of the magnetic properties returned to the original value after the permanent magnet temperature is restored, H_{ct} is intrinsic coercive force at T_t, H_{c0} is intrinsic coercive force at T_0, $\alpha_{H_{ct}}$ is

the degree of intrinsic coercive force of permanent magnets that varies reversibly with temperature.

III. The Equivalent Thermal Network Model

A. Basic assumptions

(1) The temperature distribution of SIPMSM is symmetrical along the circumferential direction, and the cooling conditions in the circumferential direction are the same;

(2) Only the copper losses, iron losses, permanent magnet eddy current losses are considered, while the impacts of other skin effects are ignored;

(3) The effect of heat radiation on the temperature field distribution is ignored.

Based on the above assumptions, the initial equivalent thermal network model and the modified equivalent thermal network model are shown in Fig. 2. The magnetic-thermal coupling is not considered in the initial equivalent thermal network model, and it is considered in the modified equivalent thermal network model. Table II shows the temperature nodes in the SIPMSM thermal network model. The two models adopt the same temperature nodes.

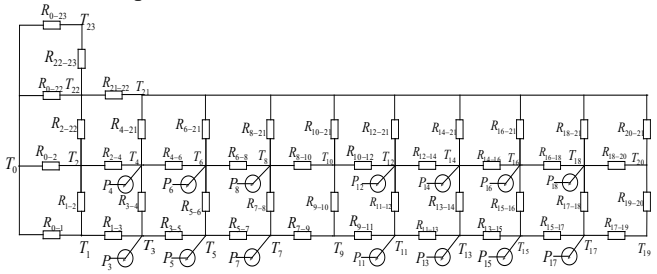

Fig. 2. The initial equivalent thermal network model.

In Fig. 2, R_{i-j} is the thermal resistance between temperature nodes i and j. P_3, P_4 denote the stator yoke iron losses. P_5, P_6 are the winding copper losses. P_7, P_8 represent the stator tooth iron losses. P_{11}, P_{12} denote the eddy current losses of SPM. P_{13}, P_{14} represent the upper rotor iron losses. P_{15}, P_{16} are the eddy current losses of IPM. P_{17}, P_{18} indicate the lower rotor iron losses.

TABLE II
TEMPERATURE NODES OF THE THERMAL NETWORK MODEL

Temperature nodes	Corresponding parts structure
T_0	External environment
T_1 、T_2 、T_{22}	Housing
T_3 、T_4	Stator yoke
T_5 、T_6	Winding
T_7 、T_8	Stator tooth
T_9 、T_{10}	Air gap
T_{11} 、T_{12}	SPM
T_{13} 、T_{14}	The upper rotor core
T_{15} 、T_{16}	IPM
T_{17} 、T_{18}	The lower rotor core
T_{19} 、T_{20}	Shaft
T_{23}	End cover

B. Thermal resistance

The size and distribution of the losses affect the temperature distribution of the motor. In the equivalent thermal network model, the loss is calculated as shown in formulas (1)-(3). According to the calculation results of formulas (1)-(3), each part of the losses is used as a heat source to be loaded into the corresponding heat source node. The heat transfer in SIPMSM mainly includes heat conduction and convection heat dissipations, neglecting the thermal radiation. The thermal resistance in SIPMSM is the conduction resistance and the convective heat dissipation, respectively, as shown in formulas (9) (10) [23]:

$$R_d = \frac{h}{\lambda_d s_d} \tag{9}$$

$$R_v = \frac{1}{\alpha_v s_v} \tag{10}$$

R_d is the conduction thermal resistance, h represents the length of heat transfer path, λ_d is the thermal conductivity, s_d denotes the conduction cross sectional area, R_v indicates the convective thermal resistance, α_v is the convection coefficient of heat transfer, s_v denotes the convection cross sectional area. R_{4-8} is taken as an example. Flat bottom slot is used to stator of SIPMSM, as shown in Fig. 3. A portion of the conductor heat in the slot is transmitted to the yoke through the bottom of the slot, and the rest to the linear portion of the stator parallel teeth. The heat exchange between the tooth portion and the yoke portion is set in the tooth width range, and the heat conduction area of the tooth portion to the yoke portion is calculated by formula (11). The thermal resistance R_{4-8} can be derived as formula (12).

$$S_{48} = b_t l_{ef} Z / 3 \tag{11}$$

$$R_{4-8} = \frac{(D_s - D_{si})/4}{\lambda_t S_{48}} \tag{12}$$

b_t represents the tooth width, l_{ef} indicates axial length, Z denotes number of pole, D_s is the stator outer diameter, and D_{si} is the stator inner diameter.

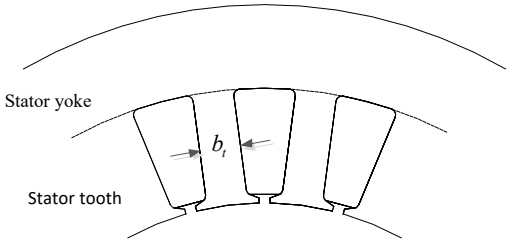

Fig. 3. The stator core section diagram.

C. Determination heat dissipation coefficient

The surface heat dissipation coefficient of SIPMSM is the parameters that reflect the surface heat of the convection heat transfer between the outer surface of housing and the surrounding air, the stator inner surface and the air gap, the rotor outer surface and the air gap. It is related to the surface temperature of the component, surrounding medium temperature, air gap medium flow rate and other factors.

Consequently, the heat dissipation coefficient of each component of SIPMSM is analyzed. In this paper, the reference temperature is chosen as 20°C.

The housing is directly in contact with the outside air, and the heat exchange between the housing and outside air takes the form of natural convection. When the air is used as the cooling medium, the heat dissipation coefficient of the housing surface depends on the air flow rate, and its coefficient of heat dissipation is expressed as shown in (13).The end surface heat dissipation coefficients of the stator and rotor cores are shown in equations (14)and(15)[24].

$$\alpha_1 = 14\left(1 + 0.5\sqrt{v_a}\right) \tag{13}$$

$$\alpha_2 = 15 + 6.5 v_r^{0.7} \tag{14}$$

$$\alpha_3 = 0.822\gamma_0 D_r^{-0.23}\left(\frac{n}{\lambda}\right)^{0.385} \tag{15}$$

Where v_a is the air blowing speed on the surface of the housing. v_r represents the linear velocity of the rotor surface. γ_0 denotes the air thermal conductivity. D_r is the rotor outer diameter. λ denotes the air viscosity coefficient. n indicates the motor speed. The air gap between the stator and rotor is affected by the tangential motion of the rotor, and the other side is blocked by the stator inner surface. Therefore, the surface heat dissipation coefficient between the stator and rotor is expressed in (16), and the surface heat dissipation coefficient at the stator winding end is shown in (17)[25].

$$\alpha_4 = 28 + 19.8 v_r^{0.5} \tag{16}$$

$$\alpha_5 = \frac{0.614\lambda_0}{D_s + D_{si}}\left[\frac{\left(D_s + D_{si}\right)}{\lambda} v_r\right]^{0.6} \tag{17}$$

Assuming the inner surface of the stator and the outer surface of the rotor are smooth and cylindrical, the equivalent coefficient of thermal conductivity of air gap within the medium can be calculated by the following methods [26]. The Reynolds number in the air gap is solved by equation (18), and the critical Reynolds number is calculated according to equation (19),

$$\mathrm{Re}_a = \frac{v_r h_a}{\lambda} = 19.55 \tag{18}$$

$$\mathrm{Re}_{cr} = 41.2\sqrt{\frac{D_{si}}{g}} = 39.3 \tag{19}$$

h_a is the air-gap thickness, and g denotes the acceleration of gravity. Because $\mathrm{Re}_a < \mathrm{Re}_{cr}$, the medium movement in the air gap is the laminar flow. Then the air gap between the stator and rotor can be regarded as ordinary air to set the coefficient of thermal conductivity.

The thermal network model is illustrated in Fig. 2, with the heat balance equations shown in formula (20), and the thermal conductivity matrix shown in formula (21), where **R** is the thermal resistance matrix, **G** denotes the thermal conductivity matrix, **T** represents the temperature nodes matrix, and **P** is the node loss matrix. The temperature node values of the SIPMSM are computed based on the equivalent thermal network method as shown in Table III.

$$\mathbf{GT} = \mathbf{P} \tag{20}$$

$$\mathbf{G} = \frac{\mathbf{1}}{\mathbf{R}} \tag{21}$$

TABLE III
CALCULATION RESULTS OF TEMPERATURE NODES FOR SIPMSM

Parameters	The initial value	The coupled value
T_0	20°C	20°C
T_1	82.8°C	84.3°C
T_3	85.1°C	86.6°C
T_5	115.9°C	117.8°C
T_7	100.2°C	101.4°C
T_{11}	94.4°C	95.8°C
T_{13}	94.1°C	95.5°C
T_{15}	94.1°C	95.6°C
T_{17}	93.3°C	94.7°C
T_{19}	93.1°C	94.4°C

IV. THE MAGNETIC-THERMAL COUPLING FINITE ELEMENT MODEL

A. Basic assumptions and calculation concept

According to the structure of SIPMSM, the motor magnetic-thermal coupling finite element model is established on the basis of the following hypothesis:

(1) The temperature field distribution of SIPMSM along the circumferential direction is symmetrical. The cooling conditions of the motor in the circumferential direction are assumed to be the same;

(2) The influence of temperature change for the steel loss is ignored and the physical characteristics of each medium in the model parameters do not change with temperature;

(3) The mechanical losses owing to the influence by temperature are ignored;

(4) Close contacts are placed between the solid components of the motor, and the influence of the junction box for the cooling is ignored;

(5) The stator slot will be stratified equivalent analysis, the equivalent model structure as shown in Fig. 4;

The magnetic-thermal coupling finite element model of SIPMSM and the flow chart of the calculation process are respectively shown in Fig. 5 and Fig. 6. The finite element application condition is to discretize the structure of SIPMSM, and the mesh adopts adaptive segmentation. The basic process of finite element method to solve the problem mainly includes: the discretization of the analysis object, the finite element solution, and the post-processing of the calculation result.

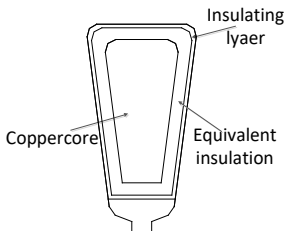

Fig. 4. The equivalent simplified model of stator slot.

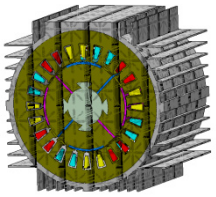

Fig. 5. The magnetic-thermal coupling finite element model of SIPMSM.

It can be seen from Fig. 7 that the relevant temperature dependent parameters are real-time updated with the change of temperature during the process of magnetic-thermal coupling step by step. According to the updated parameters, additional losses are introduced. Such an iterative computation is carried out continuously until the coupling analysis meets the requirements. The finite element model and thermal network model use the same heat dissipation coefficient.

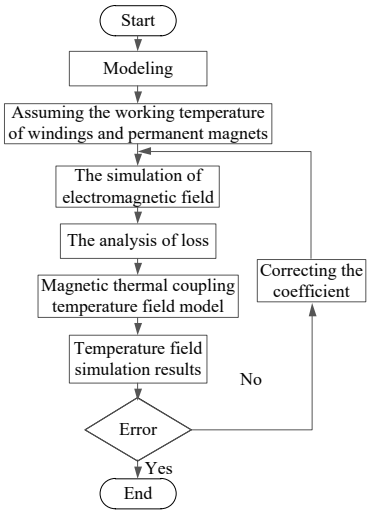

Fig. 6. Flow chart of Magnetic-thermal coupling calculation.

B. Computation results

By solving the magnetic-thermal coupling finite element model the temperature field distribution of SIPMSM in the rated operation is obtained. Table IV shows the temperatures of the main components of SIPMSM. Fig. 7 displays the three-dimensional temperature field of SIPMSM.

TABLE IV
TEMPERATURE OF MAIN COMPONENTS FOR SIPMSM

Parts of motor	The average temperature	The lowest temperature	The highest temperature
Housing	86.2°C	72.1°C	92.3°C
Stator core	93.7°C	81.5°C	107.1°C
Winding copper	120.2°C	116.3°C	123.2°C
SPM	98.4°C	98.2°C	99.7°C
Rotor core	98.3°C	96.9°C	98.9°C

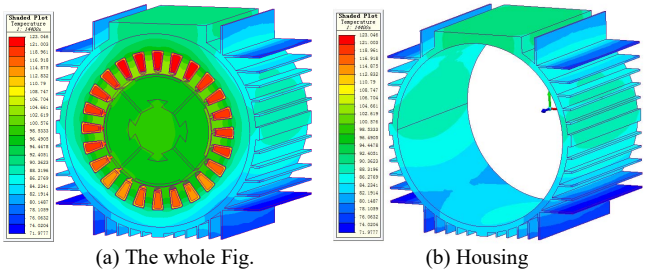

(a) The whole Fig. (b) Housing

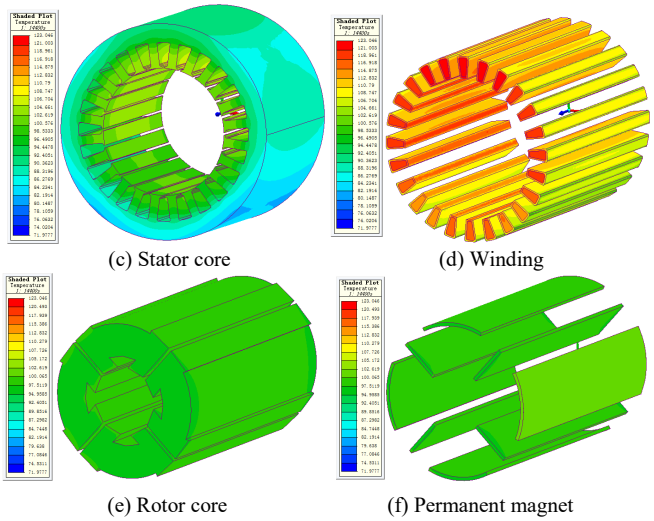

(c) Stator core (d) Winding

(e) Rotor core (f) Permanent magnet

Fig. 7. 3-D temperature field of SIPMSM at rated condition.

From the vertical comparison of Table IV, the highest temperature appears in the winding copper core, and the lowest temperature appears in the housing. From the horizontal comparison of Table 4, the temperature difference of the housing is 20.2°C, and that of the stator core is 25.6°C. The temperature differences of the SPM and rotor core are both not more than 2°C. Because the winding copper core is the main heat source and the small heat dissipation factor of the insulation layer leads to poor heat dissipation, the peak value of the temperature of SIPMSM is located at the center of the stator winding. SIPMSM is classified as a type of closed small permanent magnet synchronous motor, and the heat only radiates outward through the housing in the natural air cooling way, thus the temperature of the housing is the lowest. The eddy current losses on SPM are regarded as heat sources, so the temperature of SPM is slightly higher than that of the rotor core.

It can be seen from Fig. 7, that the temperature of the housing is unevenly distributed, since heat dissipation is faster in the areas of wind fins and lower temperature is presented in these areas. The effects of the width of fins on the temperature distributions in the housing, stator core and winding can be apparently seen in this Fig.7. The temperature difference between the rotor and stator regions is relatively large. The reason for this phenomenon is that wide fins have large areas, which is advantageous to heat dissipation of the housing. However, small thermal conductivity of the air gap leads to poor ability of heat exchange between the stator and rotor areas, and the excessive heat on the rotor is difficult to be transmitted to the stator, resulting in small overall temperature difference. A downward trend along the radial direction is presented for the temperatures of the components of the motor. The axial temperature range of housing is larger than the radial temperature range, while the situations are opposite for the other parts. The reason is that most of the heat in the motor is transferred to the stator core at first, and then it is dissipated to the surrounding air through the housing.

In order to verify the magnetic-thermal coupling method, the temperature distribution of SIPMSM with the rated operation

state is calculated by the equivalent thermal network method and the finite element method. The results are shown in Table V.

TABLE V
IN CONTRAST OF RESULTS

Parts of motor	The initial thermal network	The coupled thermal network	The coupled finite element
Housing	82.8°C	84.3°C	86.2°C
Stator core	90.1°C	92.5°C	93.7°C
Winding	115.9°C	117.8°C	120.2°C
SPM	94.4°C	95.8°C	98.4°C

C. Comparative analysis

Through comparative analysis, different calculation data of the three models is displayed, but the error is within a reasonable range. By illustrating the three models, adaptability and compatibility are presented for the temperature field calculation of SIPMSM, while validity and accuracy are guaranteed by adopting the magnetic-thermal coupling method. The magnetic-thermal coupling finite element model method is adopted. The finite element method not only has high computational accuracy, but also fully obtains the temperature field distribution and temperature curve under different operating conditions of the motor.

V. ANALYSIS OF THE TEMPERATURE FIELD IN DIFFERENT WORKING CONDITIONS

A. Rated load condition

The power supply frequency of the motor is changed and the iron loss of the motor is changed, thus it is indispensable to study the losses in the motor. The relationships among the supply frequency, iron losses and the maximum temperature of the main components of SIPMSM are shown in Fig. 8.

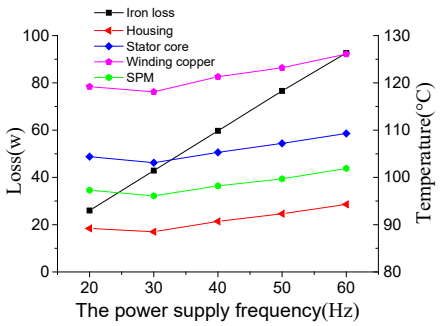

Fig. 8. Iron losses and the highest temperature of main components for SIPMSM under different power frequencies

As can be seen from Fig. 8, the iron losses increase with the increase of the power supply frequency, and the relationship between them is approximately linear. Since a constant voltage frequency ratio of the rated load is used for SIPMSM, little variation is induced in the amplitude of flux density in the core. When the power supply frequency changes, the flux density frequency of the core varies accordingly, and the iron losses are only proportionally related to the flux density frequency in this case. The simulation results are obtained by applying the finite elements show approximately linear relationships.

It can be seen from Fig. 8 that the temperatures of the main components of SIPMSM decrease first and then increase along with the increment of power supply frequency, and each of them reaches the lowest point when the power supply frequency is 30Hz. The SIPMSM operates in the low-speed operation mode when it is supplied by a power source of 20Hz with the rated load operation speed of 600rad/min. The iron losses are small in the mode, the coefficient of heat transfer and the revolving speed of motor parts are known from the formulas (14)-(17).Therefore, the heat dissipation capability will be deteriorated and the heat transfer capability between the stator and rotor will decline in when a lower speed is presented. On the contrary, the speed of the motor is high in the High-frequency operation mode. Although the heat dissipation capability is improved in this case, the iron losses increase with the increase of frequency, which also increases the temperature. Regardless of decrease or increase in the power supply frequency, the temperature of SIPMSM always increases, which indicates that the performance of SIPMSM during the frequency conversion is stable.

B. Synchronous speed condition

The temperatures of the main components of SIPMSM with respect to different loads are shown in Fig. 9.

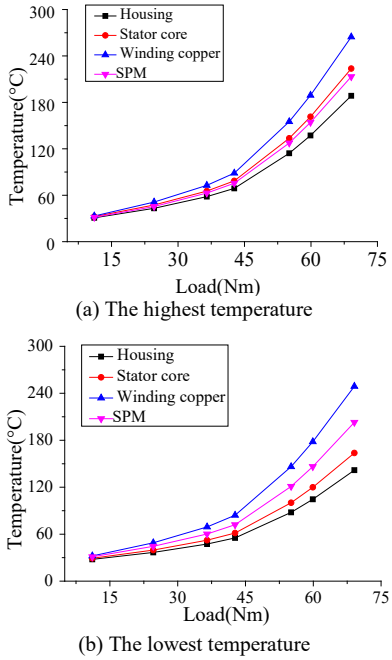

Fig. 9. Temperature of SIPMSM with different load.

It can be seen from Fig. 9 that with the increase of the load, the temperatures of the housing, stator core, winding copper core and SPM increase, but no linear relationship is presented. Instead, the slope of each graph increases with the increment of load, and among all the graphs the increase of temperature for the housing is the most moderate. The highest temperature in the motor appears in the winding copper core. It can be seen that the speed of increase for the temperature of winding copper is much higher than that of SPM and housing, which makes the overall temperature difference in the motor increasingly bigger. The reason for this phenomenon is that with the increase of load,

the stator current also increases, so the growth rate of copper losses is much greater than that of iron losses. As the main heat source, the copper core is located in the middle of the stator slot and surrounded by insulations with poor heat conduction ability. The heat dissipation capability of housing is the strongest and the change amplitude of the temperature is the smallest.

When the motor is in the full load operation mode, the highest temperature of winding copper is 123.2 °C, and the lowest temperature of housing is 72.1°C, which means that the temperature difference in the motor reaches 51.1°C. When the load torque of the motor is 55.1 Nm, the temperature of winding copper core rises sharply to 155.1°C, which is beyond the scope of class F insulation, and it will lead to rapid aging of motor insulation materials and even serious damage to the motor. When the load torque of the motor is 59.9 Nm, the temperature of the SPM drastically increases to 154.2°C, which exceeds the operating temperature of 150°C of the permanent magnet. If the operation is prolonged, it may cause irreversible demagnetization of the permanent magnet. According to the above analysis, the situation of motor overload should be prevented to avoid high temperatures in actual operations.

C. Temperature influence

The temperature of permanent magnet is important to evaluate performances of SIPMSM, and the relationship curves between the back EMF and temperature of the SPM is shown in Fig. 10(a). The relationship curves between the gap flux density and temperature of SPM is shown in Fig. 10(b).

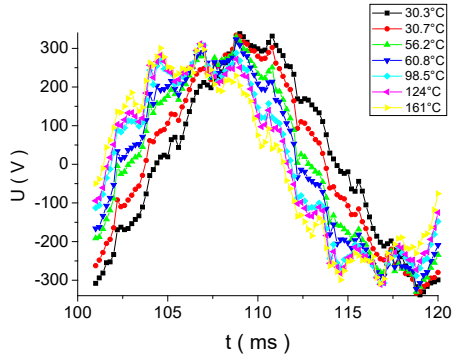

(a)The back EMF

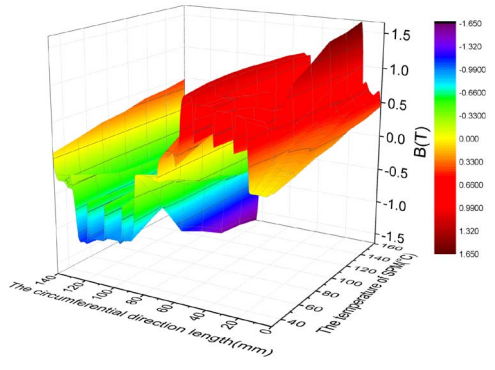

(b) The gap flux density

Fig. 10. The curves about temperature of the SPM

As can be seen from Fig. 10, with the increase of the temperature of SPM, the peak value of the back EMF is shifted and decreasing, and the peak point of the air gap flux has a skewing and decline. The main reason is that with the permanent magnet working temperature increases, permanent magnet internal remanence and coercivity are reduced, and its operating point of the shift the change of permanent magnet working temperature makes the pole of the magnetic flux and the back EMF of a certain change. Therefore, larger deviation at the working point of permanent magnet is induced, and then the back EMF produced by it is changed, which influences the distribution of the internal magnetic field of SIPMSM. The transformation of the working point of permanent magnet affects the magnetic flux densities in the air gap.

VI. CONCLUSION

By comparing the calculation results of the equivalent thermal network model and the finite element model, the conclusion is drawn that the magnetic-thermal coupling method is adaptable for calculating the temperature field of SIPMSM.

(1) The air gap makes the temperature difference between the stator region and the rotor region larger under the rated load and synchronous speed. The width of the fins has a significant effect on the temperature distribution of the stator region.

(2) The magnetic-thermal coupling mechanism is proposed, which is used to the thermal network model and the finite element model, and the accuracy of temperature field calculation is enhanced by the magnetic-thermal coupling method. The advantage in computational accuracy makes the proposed coupled analysis method efficient and practical especially in initial motor optimization design.

(3) When the power supply frequency is in the range of 20Hz-60Hz in the rated load condition, the temperature of SIPMSM is kept in the normal range, demonstrating that the working performance of SIPMSM is stable.

(4) In the synchronous speed condition, the temperature of SIPMSM is obviously affected by the load. When the motor loads 1.26 times the rated load torque, the temperature of permanent magnet begins over the limited working temperature. Therefore, the overload working state of SIPMSM should be avoided.

REFERENCES

[1] J. Si, S. He, H. Feng, et al, “Characteristic analysis of surface-mounted and interior hybrid permanent magnet synchronous motor based on equivalent magnetic circuit method,” *Journal of China Coal Society*, vol. 40, no. 5, pp. 1119-1205, 2015.

[2] J.Si,Z.Liu,M.Si,et al, “Magnetic field analysis and characteristics research on permanent magnet synchronous motors with new structure rotor,” *Journal of China Coal Society*, vol. 38, no. 2, pp. 348-352, 2013.

[3] S. He, “Modeling and Characteristic Analysis of Surface-mounted and Interior Hybrid PMSM,” M.S. thesis, *Henan Polytechnic University,* 2015.

[4] Y. Jin, W. Li and S. Li , “Numerical calculation and analysis of stator thermal field in an induction machine,” *Electric Machines and Control,* vol.10, no. 5, pp. 492-497, 2006.

[5] S. Cheng, C. Li and F. Chai, “Analysis of the 3D steady temperature field of induction motors with different cooling structures in mini electric vehicles,” *Proceeding of the CSEE*, vol. 32, no. 30, pp. 82-90, 2012.

[6] Christian Kral, Habetler T G, Harley R G, “Rotor Temperature estimation of squirrel-cage induction motors by means of a combined scheme of parameter estimation and a thermal equivalent model”. *IEEE Transactions*

on Industry Applications, vol. 40, no. 4, pp. 1049-1056, 2004.

[7] W. Li, S. Ding, H. Jin, "Numerical calculation of large synchronous generator stator temperature fields based on coupled fields," *Proceedings of the CSEE*, vol. 25, no. 13, pp. 129-134, 2005.

[8] Joo D, Cho J H, Woo K, et al, "Electromagnetic field and thermal linked analysis of interior permanent-magnet synchronous motor for agricultural electric vehicle," *IEEE Transactions on Magnetics*, vol. 47, no. 10, pp. 4242-4245, 2011.

[9] Y. Zhang, J. Ruan and T. Huang, "Calculation of temperature rise in air-cooled induction motors through 3-D coupled electromagnetic fluid-dynamical and thermal finite-element analysis," *IEEE Transactions on Magnetics*, vol. 48, no. 2, pp. 1047-1050,2012.

[10] Q. Zhang, Q. Lu, S. Huang, et al, "Temperature rise calculations of high density permanent magnet motors based on multi-domain co-simulation," *Proceeding of the CSEE,* vol. 34, no. 12, pp. 1874-1881, 2014.

[11] W. Jiang, Thomas M. Jahns, "Coupled Electromagnetic–Thermal Analysis of Electric Machines Including Transient Operation Based on Finite-Element Techniques," *IEEE Transactions on Industry Applications*, vol. 51, pp. 1880 – 1889, 2015.

[12] Jae-Bum Park, Morteza Moosavi, Hamid A, "Toliyat. Electromagnetic-thermal coupled analysis method for interior PMSM," *2015 IEEE International Electric Machines & Drives Conference (IEMDC)*, pp. 1209 – 1214, 2015.

[13] X. Zhang, W. Li and H. Qiu, "Calculation of electromagnetic field and temperature field in super high speed permanent magnet generator with composite structures," *Proceedings of the CSEE*, vol. 31, no. 30, pp. 85-92, 2011.

[14] S. Ding, F. Meng and Y. Ge, "Temperature field investigation of canned primary pump motors in nuclear power stations," *Proceedings of the CSEE*, vol. 32, no. 36, pp. 149-155,2012.

[15] Y. Lu, G. Zheng, J. Li, et al, "Uniformity of multi-path ventilation in rotor of air inner-cooled turbo generator," *Proceedings of the CSEE*, vol. 30, no. 3, pp. 99-104, 2010.

[16] S. Ding, B. Guo, H. Feng, et al, "Temperature field investigation of permanent magnet synchronous motors controlled by the frequency conversion control system," *Proceedings of the CSEE*, vol. 34, no. 9, pp. 1368-1375, 2014.

[17] Y. Huang, Q. Hu, J. Zhu, "Magnetic-Thermal Analysis of a High-Speed Claw Pole Motor Considering Rotational Core Loss," *Transactions of China Electrotechnical Society*, vol. 25, no. 5, pp. 54-60, 2010.

[18] W. Li, X. Yang, D. Gu, et al, "Calculation and analysis of fluid flow and heat transfer of air-cooled turbo-generator with multipath ventilation," *Transactions of China Electrotechnical Society*, vol. 24, no. 12, pp. 24-31, 2009.

[19] Y. Xu, Z. Jiang, M. Ai, "Coupling characteristics research on electromagnetism and temperature and force of the magnetic isolated segment in the submersible motor," *Transactions of China Electrotechnical Society*, vol. 30, no. 15, pp. 172-178, 2015.

[20] J. Si, L. Zhang, H. Feng, et al, "Analysis of 3-D temperature field for a surface-mounted and interior permanent magnet synchronous motor," *Electric Machines and Control*, vol. 21, no. 3, pp. 25-31, 2017.

[21] W. Zhu, "Research on rotor magnet loss thermal field in permanent magnet synchronous motor for electric vehicles," Ph.D. dissertation, *Beijing institute of technology*, 2014.

[22] R. Tang, "Theory and design of modern permanent machine," book, 1st edition, China Machine Press, Beijing 2015, pp.19-20.

[23] X. Wang, P. Gao, "Application of Equivalent Thermal Network Method and Finite Element Method in Temperature Calculation of in-Wheel Motor," Transactions of China electrotechnical society, vol. 31, no. 16, pp. 26-33, 2016.

[24] G. Huang, F. Fu, "Small and medium-sized motor design manual," book, 2nd edition, China Electric Power Press, Beijing 2014, pp.434-447.

[25] T. Hu, R. Tang, Y. Li, et al, "Thermal analysis and calculation of permanent magnet wind generator," Transactions of China electrotechnical society, vol. 28, no. 3, pp. 122-126, 2013.

[26] Y. Tai, Z. Liu, "Analysis on Three-dimensional transient temperature field of induction motor," Proceeding of the CSEE, vol. 30, no. 30, pp. 114-120, 2010.

Jikai Si received the B.S. degree in electrical engineering and automation from the Jiaozuo Institute of Technology, Jiaozuo, China, in 1998; the M.S. degree in electrical engineering from Henan Polytechnic University, Jiaozuo, China, in 2005; and the Ph.D. degree in 2008 from the School of Information and Electrical Engineering, China University of Mining and Technology, Xuzhou, China, in 2008.

He is currently a professor at Henan Polytechnic University. His main research interests include the theory, application, and control of special motor. He has authored and co-authored over 90 technical papers in these areas.

Dr. Si is a Member of the Institute of Linear Electric Machine and Drives, Henan Province, China.

Suzhen Zhao received B.S. degree from Henan Polytechnic University, Jiaozuo, China, in 2015.

She is currently pursuing the M.S. degree in electrical engineering.

Her research interests include modeling and characteristic analysis of special motors

Haichao Feng received the B.S. and M.S. degrees in electrical engineering and automation, control theory, and control engineering from the School of Electrical Engineering and Automation, Henan Polytechnic University, Jiaozuo, China, in 2005 and 2008, respectively.

He is a Teacher at the School of Electrical Engineering and Automation, Henan Polytechnic University. In recent years, he has participated in eight provincial and three country research projects, and has published more than eight academic papers. His research interests include the optimization design of linear and rotary machines, power electronics, and their controls.

Yihua Hu (M'13–SM'15) received the B.S. degree in electrical motor drives and the Ph.D. degree in power electronics and drives from the China University of Mining and Technology, Jiangsu, China, in 2003 and 2011, respectively. From 2011 to 2013, he was with the College of Electrical Engineering, Zhejiang University, as a Postdoctoral Fellow. From 2012 to 2013, he was an Academic Visiting Scholar with the School of Electrical and Electronic

Engineering, Newcastle University, Newcastle upon Tyne, U.K. From 2013 to 2015, he was a Research Associate with the Power Electronics and Motor Drive Group, University of Strathclyde. He is currently a Lecturer with the Department of Electrical Engineering and Electronics, University of Liverpool. He has published over 60 peer-reviewed technical papers in leading journals. His research interests include PV generation system, power electronics converters and control, and electrical motor drives.

Wenping Cao(SM'11) received the B.Eng. degree in electrical engineering from Beijing Jiaotong University, Beijing, China, in 1991, and the Ph.D. degree in electrical machines and drives from the University of Nottingham, Nottingham, U.K., in 2004. He is currently a Chair Professor of Electrical Power Engineering and the Head of Power Electronics, Machines and Power System Group with Aston University, Birmingham, U.K. Dr. Cao is currently a Royal Society Wolfson Research Merit Award holder, U.K. He was a semifinalist at the Annual MIT-CHIEF Business Plan Contest, USA, in 2015; the Dragon's Den Competition Award winner from Queen's University Belfast, U.K., in 2014; and the Innovator of the Year Award winner from Newcastle.